*Friction* **1**(1): 72–80 (2013)
DOI 10.1007/s40544-013-0006-2 ISSN 2223-7690
RESEARCH ARTICLE

# Adhesive and corrosive wear at microscales in different vapor environments

**Sihan SHEN, Yonggang MENG***
*State Key Laboratory of Tribology, Tsinghua University, Beijing 100084, China*
*Received: 24 December 2012 / Revised: 18 February 2013 / Accepted: 20 February 2013*
© The author(s) 2013. This article is published with open access at Springerlink.com

**Abstract:** Adhesive and corrosive wear at microscales are quantitatively distinguished in lifetime tests of resonant bulk-fabricated silicon microelectromechanical systems (MEMS). By analyzing the oscillation decay characteristics in different vapor environments, we find that wear is dominated by asperity adhesion during the initial stages of rubbing in dry $N_2$ or $O_2/N_2$ mixtures; in these situations the transient wear rate is inversely proportional to the wear depth. But in water or ethanol vapors, chemical reactions between the corrosive adsorbed layer and the silicon substrate limit the wear rate to a constant. These observations are consistent with atomic explanations. The differences between adhesive and corrosive wear explain the advantages offered by lubricating with alcohol vapors rather than using dry environments for tribo-MEMS devices. Compared to ethanol, the relatively poor anti-wear effect of water vapor is explained by aggressive and rapid tribo-reactions.

**Keywords:** adhesive wear; corrosive wear; microelectromechanical systems (MEMS)

## 1 Introduction

Depending on the working environment, wear may be a process that is not only mechanical but also chemical. With the progress in atomic force microscopy (AFM) and tribo-microelectromechanical systems (MEMS), wear has been studied at nano- and microscales in situations where the wear mechanism can be altered by changing the chemical environment in the same contact system.

Single asperity wear has been widely researched using AFM. In inert environments, such as ultrahigh vacuum or nitrogen atmospheres, wear shows purely mechanical origins that vary from atom migration [1] to adhesive features [2]. But when exposed to air, AFM tips usually suffer oxidation wear in which the oxide layer, rather than the substrate itself, is worn off [2]. When a tip is immersed in an aqueous solution [3, 4], wear occurs on a layer of chemical precursor formed on the rubbing area. However, due to the lack of quantitative methods, wear mechanisms of MEMS devices (in which wear usually occurs on multi-asperity contacts [5, 6]) in different environments are still not well understood. Miller et al. analyzed the wear morphologies of surface-fabricated microgears and suggested that, from among seven primary wear mechanisms, adhesive wear is the most likely explanation for failures occurring in air environments [7]. In addition, the influence of environmental humidity has been studied by examining post-wear morphologies. Unlike high-vacuum environments, dry air (relative humidity (RH) <1%) can passivate nascent surfaces to avoid cold welding between silicon asperities [8]. At increased moisture contents (35%–50% RH), air is considered to be an anti-wear lubricant that reduces wear debris [9, 10].

This suggests that, to enable tribo-MEMS to operate over long durations, their chemical environments need to be carefully designed. Perfluorodecanoic acid vapor has been used for protecting aluminum protrusion in the Digital Micromirror Device™ [11], and 1-pentanol vapor has been shown to be effective in prolonging

* Corresponding author: Yonggang MENG.
E-mail: mengyg@mail.tsinghua.edu.cn

the lifetime of the silicon micro-tribotester fabricated by Sandia National Laboratory [12]. To develop new applications of MEMS, an understanding of wear mechanisms at microscales becomes particularly important.

Both direct observations of rubbing surfaces and analyses of frictional force signals provide hints about wear mechanisms. By using direct observations, wear patterns at key running-time nodes during wear evolution are scanned by AFM [1, 13, 14], Auger electron spectroscopy [14], transmission electron microscope [15], or scanning electron microscopy (SEM) [6, 16]. These geometric measurements lead to intuitive speculations about wear mechanisms. However, this approach places high demands on sample preparation. Further, direct observation would not even be possible when the rubbing area is deeply hidden in the test pair or when the wear evolution is so rapid that it cannot be sampled by interrupted testing. In such cases, the wear mode could be inferred by analyzing the characteristics of frictional and adhesive forces developed with the sliding length and/or normal load [4, 17, 18]. This purpose can be met by MEMS tribometers equipped with a function for friction-force measurements.

To study wear mechanisms at microscales, a bulk-fabricated sidewall Si-MEMS tribotester was fabricated and used to compare tribological behaviors in different vapor environments. The oscillation of a resonant mass was controlled by friction, and the decay of the oscillation was analyzed using a simplified dynamic equation. Adhesive and corrosive wear were distinguished by analyzing differences in the oscillation decay mode. We first introduce the experiment and oscillation model, and then we give an atomic perspective of environment-related wear mechanisms. In the last section we discuss the benefits of vapor-phase lubrication for prolonging the lifetime of tribo-MEMS.

## 2 Experiments

The Si-MEMS tribotester has two 50-μm-thick friction pairs with a 1 mm × 1 mm driving shuttle (Fig. 1(a)) in common. Each friction pair consists of a loading frame and a restriction beam. The restriction beam is connected to the driving shuttle and moves perpendicularly to the loading direction. The loading frame can be pushed by an external tungsten tip via a buckle mechanism over a certain displacement to maintain the deflection of the restriction beam. The stiffness of the restriction beam is 1.58 N/m; there are two stages of pushing displacement to realize normal loads of 2.7 μN and 5.2 μN. This design avoids the necessity of finding the zero-point with a trial way before the wear test; consequently, it protects the initial surface topology from unexpected damages. The two mirrored friction pairs can cancel chip inconsistency [19] to compare the anti-wear effects of different vapors.

The standard Bosch process was used to release the Si-MEMS tribotester, which floats on a 0.5-mm-thick glass substrate. For high-frequency rubbing, the back of the glass substrate was glued to a home-made one-dimensional piezoelectric platform; this forces the driving shuttle to vibrate at a frequency close to its first-order resonance. The vibrational amplitude of the platform is less than 0.23 μm, and the typical oscillation of the shuttle is about 4.5 μm under the unloaded condition. A HeNe 633-nm laser beam was focused on the edge of the shuttle to reflect a speckle field (Fig. 1(b)), and a steady point inside this speckle field was measured with a light intensity meter. Since the shape of the speckle field is determined by the location of the shuttle edge, the intensity of the steady point can be used to detect the shuttle position. The theoretical limit of displacement resolution with the method is estimated to be 60 nm. The local vapor environment around the friction pair during tests was maintained by a 120 mL/min flow of dry nitrogen (purity > 99.5%); of this flow, 45 mL/min was bubbled through a liquid column to carry water or ethanol (denoted as 45:75).

In each test, the following steps were performed. (1) Carefully adjust the optical arrangements and choose a suitable steady point to ensure a linear correspondence between the output of the intensity meter and the displacement of the driving shuttle. (2) Tune the driving frequency (3500–4000 Hz) so the shuttle oscillation is about 4.5 μm on the microscope. (3) Record the output of the light intensity meter for oscillations in the load-free condition. (4) Push the buckle using a tungsten tip to load the restriction beam (Fig. 1(c)). (5) Immediately restart the piezoelectric platform and make the test shuttle vibrate until it

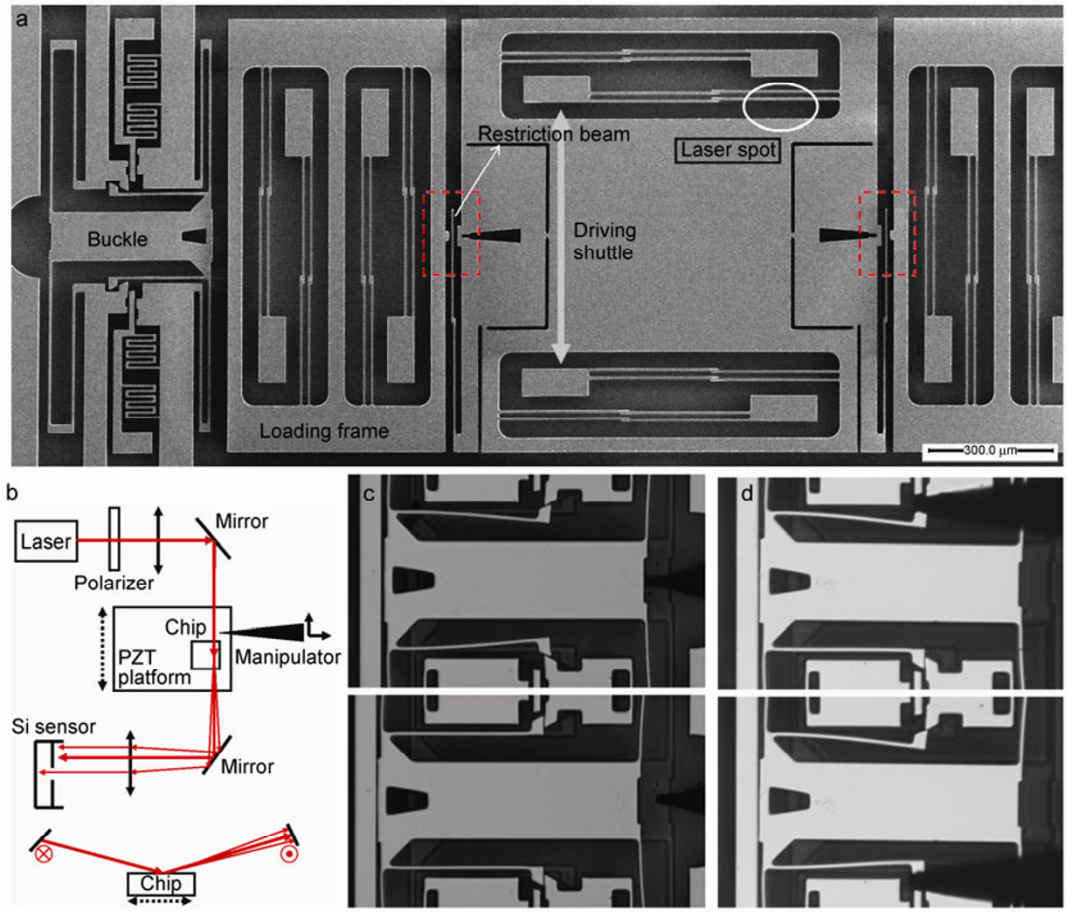


**Fig. 1** (a) The structure of the micro-fabricated tribotester. The two friction pairs are denoted by red boxes. (b) The optical path to measure the displacement of the driving shuttle, top view (up) and side view (down). (c) Load the restriction beam by pushing the buckle mechanism with tungsten tip. (d) Release the buckle mechanism after the wear test.

stops spontaneously. (6) Release the buckle mechanism (Fig. 1(d)) using the tungsten tip to unload the restriction beam for preparing the pair test. (7) Push the buckle in the opposite direction to load the neighboring test shuttle and then repeat the vibration test in alternated vapor condition.

## 3 Oscillation model of the driving shuttle

The dynamic behavior of the driving shuttle was modeled as a mass-spring-damping system. The linear stiffness of the supporting cantilever is $k = 8 \times Ez(b/l)^3$ (70 N/m), where $E$ is Young's modulus, $z$ is the cantilever height, $b$ is the cantilever width, and $l$ is the cantilever length. However, nonlinear stiffness must be considered since the oscillation amplitude $C$ is close to the cantilever width $b$ (6 μm). An effective way to calculate the total spring force is to assume the cantilever still obeys the linear deformation rule and calculate the work done by the tensile force along the cantilever axis. Therefore, the total elastic work is in the form of $x^2 + x^4$, where $x$ is the displacement of the driving shuttle. Then the total spring force is expressed by $kx + k_3x^3$ where the nonlinear stiffness coefficient $k_3$ is $8 \times (9/25)\, Ezb/l^3$ (0.7 μN/μm$^3$), which is consistent with the stiffness calibration results. To measure the damping ratio $\xi$, the driving shuttle was excited to a stable vibration, and then the platform was shut off to record the oscillation degradation. During this decay process, the dynamic equation is simply $m\ddot{x} + 2\xi\omega_0 m \cdot \dot{x} + kx + k_3x^3 = 0$, where $m$ is the shuttle mass and $\omega_0$ ($= \sqrt{k/m}$) is its natural frequency. This degradation can be fitted by the approximate solution $x = x_0 e^{-\xi\omega_0 t}$ [20] to obtain the value of $\xi$. Tests with four initial

amplitudes $x_0$ ranging from 2.84 μm to 6.50 μm confirm that $\xi$ is independent of the velocity and is less than 0.0007. Accordingly, the linear damping force is less than 0.5 μN, which is about 1/20 of the maximum time-averaged frictional force. Hence the linear damping force is omitted from the following analysis.

Thus the dynamic equation for the driving shuttle during a wear test can be written as

$$m\ddot{x} + \rho \cdot \mathrm{sgn}(\dot{x}) + kx + k_3 x^3 = kD_1 \sin(\omega t) + kD_2 \cos(\omega t) \tag{1}$$

where $D = \sqrt{D_1^2 + D_2^2}$ is the vibration of the platform and $\omega$ is the driving frequency in the monostable region (about 3800 Hz). Here we use Coulomb damping to express the frictional force with a slowly changing intensity $\rho$. To probe the friction directly, the driving shuttle can be loaded by a 1972 N/m sensor beam with a natural frequency of 190 kHz; this beam bends linearly in response to friction. Since the friction distribution is almost uniform over time, $\rho$ can be regarded as the time-averaged frictional force over a few cycles of oscillation. To avoid a rigorous discussion of the model's validity during time intervals shorter than one driving cycle, the measured vibrational amplitude was averaged over every five cycles.

Though the dynamic system includes two nonlinear terms, sgn($\dot{x}$) and $x^3$, the measured movement of the driving shuttle was still sinusoidal. Therefore $x(t) = C\sin(\omega t)$ was used as the approximate solution, and $C$ was taken to be a time-averaged, slowly changing amplitude, analogous to $\rho$. To fix the sign of the $\rho$ term, we define the residual of Eq. (1) to be $I(t)$ and consider these two integrals: $\int_{-\pi/2\omega}^{\pi/2\omega} I\mathrm{d}t$ and $J(a) = \int_a^{a+\delta} I\mathrm{d}t$, where $\delta$ is a small constant. To make the first integral vanish, $D_2$ must equal to $\pi\rho/2k$. To make the second integral vanish, we must have

$$\begin{aligned}\frac{\partial J}{\partial a} = {} & \frac{\pi\rho}{2}(\cos(\omega a) - \cos(\omega(a+\delta))) \\ & + (D_1 k - Ck + Cm\omega^2 - \frac{3}{4}C^3 k_3)(\sin(\omega a) - \sin(\omega(a+\delta))) \\ & + \frac{1}{4}C^3 k_3(\sin(3\omega a) - \sin(3\omega(a+\delta))) \\ = {} & 0\end{aligned} \tag{2}$$

where only the $D_1$ term can be zero. Using $D_1^2 + D_2^2 = D^2$, the relationship between $C$ and $\rho$ is

$$\left(C\left(1 - \left(\frac{\omega}{\omega_0}\right)^2\right) + \frac{3}{4}\frac{k_3}{k}C^3\right)^2 + \left(\frac{\pi\rho}{2k}\right)^2 = D^2 \tag{3}$$

In the empty load situation Eq. (3) becomes

$$\left(C_0\left(1 - \left(\frac{\omega}{\omega_0}\right)^2\right) + \frac{3}{4}\frac{k_3}{k}C_0^{\,3}\right)^2 = D^2 \tag{4}$$

Substituting Eq. (4) into Eq. (3) and rounding the quadratic term of $\Delta C$ ($C_0$–$C$), $\rho$ is eventually obtained in terms of $\Delta C$ as

$$\rho = \Lambda \cdot k\sqrt{C_0 \Delta C} \tag{5}$$

A more rigorous analysis gives the same form, where $\Lambda$ = 0.09 is a dimensionless apparatus constant. Here $k$ and $C_0$ are isolated from $\Lambda$ to compensate for chip inconsistencies caused by uncertainties in fabrication. Equation (5) implies that friction is zero when the vibrating shuttle does not decay, and that the magnitude of the decay is proportional to the square of the frictional force.

## 4 Wear mechanisms

After starting the wear test, the oscillation amplitude $C$ gradually degraded from its empty-load value $C_0$ to zero over a time period $t_1$, i.e., a sudden jump to stick. The time interval $t_1$ is defined as the lifetime of the tribotester; depending on sample and test conditions, the lifetime lasted from less than one second to a few minutes. Figure 2 shows several typical records of $\Delta C$ in different vapor environments. Two transient modes of $\Delta C$ were observed. The first type (Type Ⅰ) appears in dry $N_2$ or in $O_2/N_2$ mixtures (25:75); in Type Ⅰ mode, $\Delta C$ displays a transient increase at the beginning and then it remains almost stable until a sudden failure occurs. The strong variations in the plot imply lack of lubrication; if the variations are digitally filtered out, the initial increase has an approximately linear form. That is, $\rho$ is proportional to $\sqrt{t}$. The second type of mode (Type Ⅱ) was observed in environments of moist air (10%–15% RH), water vapor, and ethanol vapor. In these situations,

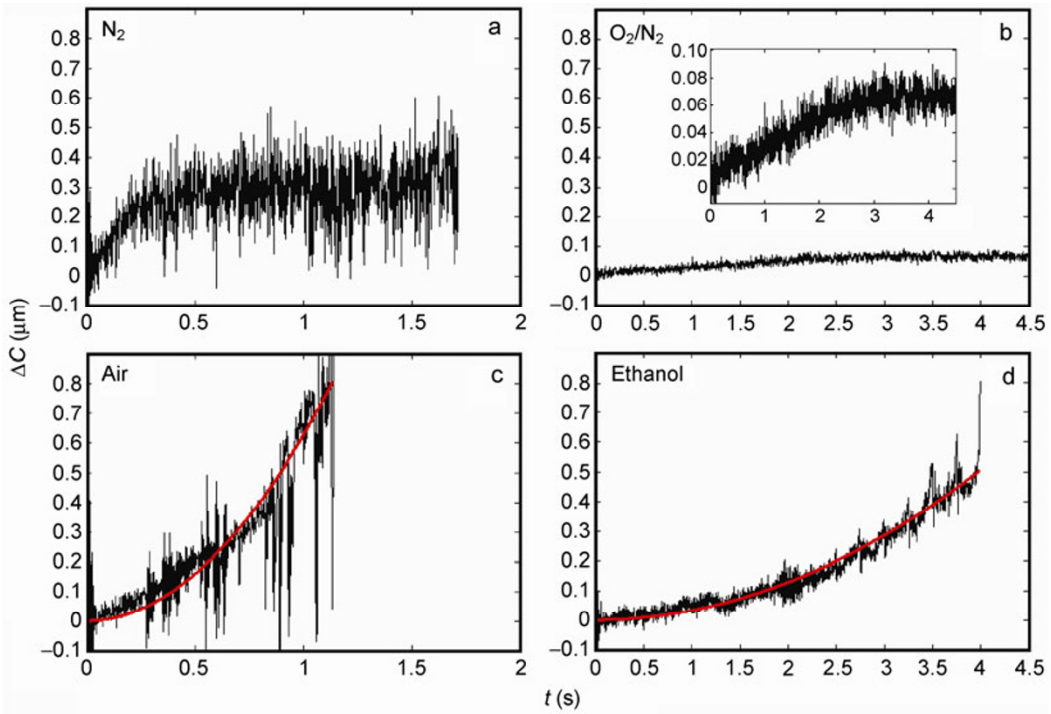


**Fig. 2** Typical increasing modes of $\Delta C$ in (a) dry nitrogen, (b) $O_2/N_2$ mixture (25:75), (c) moist air (about 10% RH), and (d) ethanol vapor (45:75) environment, where the measured vibration amplitude is averaged every five cycles. $\Delta C = d \cdot t^2$ (red line) is used to fit the data in air and ethanol vapor situations.

$\Delta C$ always shows quadratic growth ($\rho$ increases linearly with time). In addition, fluctuations were observed in the air environment.

These mesoscopic tribo-behaviors can be understood at the atomic level in the framework of classical tribology. Assuming each asperity has a parabolic shape, then $h = r_0 \cdot r^2$ ($h$ = the asperity height or wear depth, $r$ = distance from the center of the asperity tip, $r_0$, a factor describing the curvature of the asperity tip), and the average frictional force $\rho$ is proportional to the total bearing area $A = N \cdot A_0 = N(\pi \cdot h / r_0)$ where $N$ denotes the total number of asperity-asperity contacts. Wear happens when the energy dissipated at the surface is enough to destroy chemical bonds between silicon atoms. In nitrogen environments, adsorbed $N_2$ molecules could not passivate dangling bonds on Si atoms induced by rubbing effects. These atoms can form Si–Si bridges between counter surfaces. Meanwhile, silicon is chemically sensitive to $O_2$ in tribo-conditions [21]. However, because of lacking saturating radicals, such as –H or $–CH_3$, oxidized surface layers can still form dangling bonds, such as –O-Si· and –Si-O·. So in Type Ⅰ environments, counter surfaces are connected by unsaturated atoms to cause adhesive wear, just as in macroscale situations. The Archard wear equation is [18, 22]

$$\frac{A \cdot \Delta h}{v \cdot \Delta t} = \frac{\Delta V}{\Delta s} = \lambda_1 A_r \tag{6}$$

where $V$ is the wear volume, $s$ is the sliding length, $v$ is the sliding speed, and $\lambda_1$ is the wear coefficient. Combining Eq. (6) with the simplified relationship between atomic contact area $A_r$ and normal load $F_n$, $A_r = \lambda_2 \cdot F_n$ [23], the transient wear rate is found to be inversely proportional to the wear depth.

$$\frac{\mathrm{d}h}{\mathrm{d}t} = \lambda_1 \lambda_2 v \frac{F_n}{A} = \left( \frac{\lambda_1 \lambda_2 v \cdot r_0}{\pi \cdot N} \right) \frac{F_n}{h} \tag{7}$$

Equation (7) induces $h \propto \sqrt{t}$ or $\rho \propto \sqrt{t}$, which are consistent with the results in initial stages of Type Ⅰ environments. Moreover, without lubrication, tiny wear debris may gradually accumulate on the bearing area to separate counter surfaces; this would lead to the almost flat stage of $\Delta C$.

But when a dissociating compound such as water [24] (with end group –H) or ethanol [25] (with end group $–CH_2CH_3$) fully adsorbs on the rubbing surface, instead of forming dangling bonds, these molecules react with silicon atoms [26] to maintain their saturated structures and eliminate direct interactions between counter surfaces. In such situations, only the reacted atoms are worn out and the wear rate $h_0$ obeys the Arrhenius law:

$$h_0 = \frac{\mathrm{d}h}{\mathrm{d}t} = d_a K \cdot f_0 \exp[-(E_a - \Delta E)/k_B T] \quad (8)$$

where $d_a$ represents the silicon atom diameter. Unlike AFM experiments with well-defined wear asperity, we introduce a probability multiplier $K$ into Eq. (8) to express the uniform assignment of multi-contact wear. In Eq. (8) $E_a$ is the equivalent reaction barrier of $H_2O$ or ethanol with Si in a spontaneous situation. Since asperities in engineering surfaces are blunter (top radius > 20 nm) than AFM tips, the shear-induced modification $\Delta E$ can be considered to be independent of $F_n$ [17]. Therefore, if strong chemical reactions occur on the rubbing surface, the wear rate $h_0$ is a time-independent constant, which induces $h = h_0 \cdot t$ or $\rho \propto t$, consistent with the results in Type Ⅱ environments. The reacted layer is usually easier to shear than the silicon material, thereby providing positive effects both on lubrication and wear resistance: (1) this layer works as a lubricating film [27] to smooth oscillations, and (2) wear always happens on such a layer and the wear rate is limited by the tribo-reaction.

This wear model can be further tested by investigating the relationship between $h_0$ and $t_l$ in experiments using Type II environments. Using Eq. (8), the average frictional force $\rho$ and the dimensionless wear volume $r_0^2 S$ ($S$ is the cross area of the worn asperity) are both functions of $h_0 \cdot t$. No matter whether the device fails due to excessive friction or to wear, $h_0 \cdot t_l$ should be a constant if the tribological failure criterion really exists. For all experiments in Type Ⅱ environments, $\Delta C$ can be fitted by $\Delta C(t) = d \cdot t^2$. By considering $\rho = \lambda \cdot N(\pi \cdot h_0 t / r_0)$ and using Eq. (5), $h_0$ equals $(\Lambda/\lambda\pi)(r_0/N) \cdot k\sqrt{C_0 d}$, where $\Lambda/\lambda\pi$ and $r_0/N$ are regarded as constants for all samples. Figure 3 shows the relationship between $t_l$ and $k\sqrt{C_0 d}$ for thirteen samples under different vapor conditions and normal loads. This figure confirms the inverse relation between $h_0$ and $t_l$, implying that all failures are related to the same fundamental tribological mechanism.

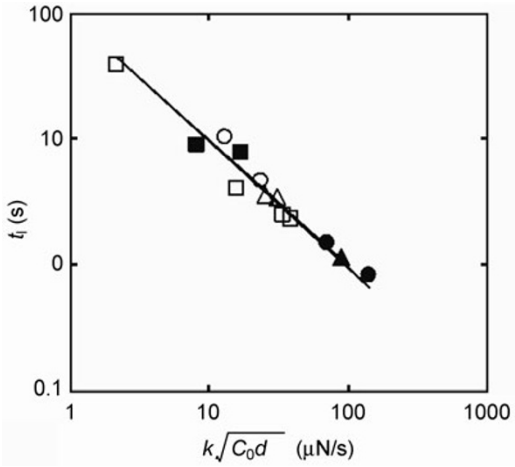


**Fig. 3** The relationship of $t_l$ and $k\sqrt{C_0 d}$ in Type Ⅱ environment. The line is fitted by $\lg t_l = -\lg k\sqrt{C_0 d} + 1.99$ (±0.10, 1$\sigma$). ○●, water vapor (45:75); △▲, moist air (10%–15% RH); □■, ethanol vapor (45:75). Solid symbol, the normal load is 5.2 μN ± 0.8 μN; open symbol, the normal load is 2.7 μN ± 0.7 μN.

Figure 4 shows SEM images of worn morphologies of loading heads and restriction beams that failed in nitrogen and ethanol vapor environments. On restriction beams (Figs. 4(a) and 4(b)), only blunt peaks can be seen. However, on loading heads (Figs. 4(c) and 4(d)), the worn areas concentrate in a small region of less

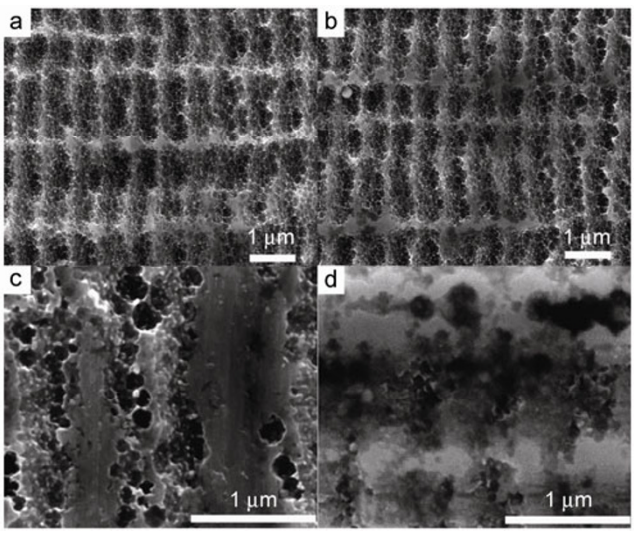


**Fig. 4** Worn morphologies of driving shuttles (a, b) and loading heads (c, d) after device failure. (a, c) Dry nitrogen atmosphere. (b, d) Ethanol vapor environment.

than 5 μm × 5 μm with more wear features. For samples in nitrogen atmospheres (Fig. 4(c)), scratches and pie-like wear debris were distributed on the wear scars, while glass-like materials around bearing spots without scratches were found on samples working in ethanol vapor atmospheres (Fig. 4(d)). These glass-like materials can decompose in wet hydrofluoric acid vapor and are considered to be the reaction products of silicon and ethanol in rubbing conditions. Therefore, though the real morphologies are quite complex, wear in nitrogen is adhesive while in ethanol vapor it is corrosive.

## 5 Discussion

The scaling of oscillation amplitude versus duration time reflects intrinsic differences between adhesive and corrosive wear mechanisms. It also provides a practical way to judge wear types at microscales. Besides the simple adhesive and corrosive situations, it can be used to recognize more complex wear patterns. For instance, Fig. 5 shows the oscillation decay in a 2,2,2-trifluoroethanol ($CF_3CH_2OH$) vapor environment. According to a first principle calculation, 2,2,2-trifluoroethanol can react with silicon in a manner similar to ethanol, but with a higher potential energy barrier (about 16.3 kJ/mol). Therefore, at the start of the wear test, adhesive wear is the dominant mechanism to blunt fresh asperities and $\Delta C$ exhibits a linear increase, while the chemical effect can appear only on a relative smoother surface in the second half.

The differences between adhesive and corrosive wear allow us to explain the benefits of vapor-phase lubrication [12] for tribo-MEMS, where an alcohol (ethanol, propanol, pentanol, etc.) is vaporized to passivate rubbing surfaces. For adhesive wear, Eq. (7) shows that the dimensionless wear volume $r_0^2 S$ is proportional to $t^{3/4}$, while in corrosive wear, it is proportional to $t^{3/2}$. Though $t^{3/2}$ has a super linear increase when the running time is long, it grows slower than $t^{3/4}$ in the early stage. Therefore, as long as the critical wear volume is not large, the adhesive situation will reach the failure point first. According to Figs. 4(a) and 4(b), for both dry nitrogen and ethanol vapor conditions, the total bearing areas on the sidewalls of the restriction beam were only 3%–6% of the nominal contact region. By comparing with the out-of-chip test during the period from 5 s to 300 s [28], samples in the lifetime test failed during the initial stage of wear evolution. Consequently, if suitable chemical reactions have been introduced on the rubbing surface, the wear process can be suppressed to a lower level than the adhesive cases, thereby prolonging the lifetime.

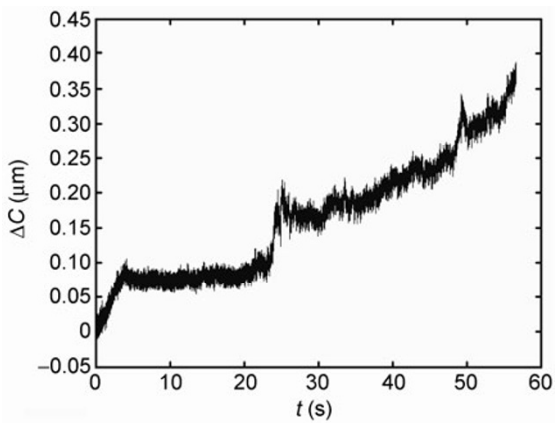


**Fig. 5** The increasing mode of $\Delta C$ in $CF_3CH_2OH$ environment.

Since water can mono-adsorb on silicon surfaces when the RH is more than 30% [29], moist air was once considered to be vapor-phase lubricant [9, 10]. But modern vapor-phase lubrication uses alcohol, instead of water. In tests comparing ethanol to water/10%–15% RH air, the lifetime $t_l$ of the latter is no more than one fifth of the former. According to the corrosive wear model, $h_0$_water is larger than $h_0$_ethanol, resulting in an earlier arrival at the failure criterion. Since tribo-chemistry is a complicated process with multiple steps, such a single-step analysis [30] may not give a correct estimate of $E_a$ in Eq. (8). Here the experimental results confirm that, without alkyl groups, water has a larger equivalent reaction rate from the experimental point of view. This means that if a chemical reaction is introduced into the tribo-system to control wear at microscales, the reactivity should be carefully verified. Aggressive rapid reactions may not lead to low wear rates.

## 6 Conclusions

Two different wear mechanisms, adhesive and corrosive, corresponding to different chemical environments

were quantitatively distinguished at microscales. This was accomplished by analyzing the oscillation behavior in lifetime tests of a bulk-fabricated Si micro-tribotester. In dry $N_2$ or $O_2/N_2$ mixtures, wear is dominated by adhesion, with the transient wear rate being inversely proportional to the wear depth. But when water or ethanol vapors are introduced into the environment, chemical reactions limit the wear rate to a constant. For engineering applications, vapor-phase lubrication for tribo-MEMS devices can reduce the wear rate in the early stages of wear processes, and chemical reactions should be controlled to a proper intensity to passivate nascent surfaces and avoid unexpected corrosion.

## Acknowledgements

This work was supported by the National Natural Science Foundation of China (NSFC, Nos. 91123033 and 51021064).

**Open Access:** This article is distributed under the terms of the Creative Commons Attribution Noncommercial License which permits any noncommercial use, distribution, and reproduction in any medium, provided the original author(s) and source are credited.

## References

[1] Gnecco E, Bennewitz R, Meyer E. Abrasive wear on the atomic scale. *Phys Rev Lett* **88**: 215501–215504 (2002)

[2] Chung K H, Lee Y H, Kim D E. Characteristics of fracture during the approach process and wear mechanism of a silicon AFM tip. *Ultramicroscopy* **102**: 161–171 (2005)

[3] Katsuki F, Kamei K, Saguchi A, Takahashi W, Watanabe J. AFM studies on the difference in wear behavior between Si and $SiO_2$ in KOH solution. *J Electrochem Soc* **147**: 2328–2331 (2000)

[4] Maw W, Stevens F, Langford S C, Dickinson J T. Single asperity tribochemical wear of silicon nitride studied by atomic force microscopy. *J Appl Phys* **92**: 5103–5109 (2002)

[5] Tanner D M, Miller W M, Peterson K A, Dugger M T, Eaton W P, Irwin L W, Senft D C, Smith N F, Tangyunyong P, Miller S L. Frequency dependence of the lifetime of a surface micromachined microengine driving a load. *Microelectronics Reliability* **39**: 401–414 (1999)

[6] Subhash G, Corwin A D, de Boer M P. Evolution of wear characteristics and frictional behavior in MEMS devices. *Tribol Lett* **41**: 177–189 (2011)

[7] Miller W M, Tanner D M, Miller S L, Peterson K A. MEMS reliability: The challenge and the promise. In *Proceedings of 4th Annual 'The Reliability Challenge'*, Dublin, Ireland, 1998: 41–47.

[8] Patton S T, Zabinski J S. Failure mechanisms of a MEMS actuator in very high vacuum. *Tribol Int* **35:** 373–379 (2002)

[9] Patton S T, Cowan W D, Eapen K C, Zabinski J S. Effect of surface chemistry on the tribological performance of a MEMS electrostatic lateral output motor. *Tribol Lett* **9**: 199–209 (2000)

[10] Tanner D M, Walraven J A, Irwin L W, Dugger M T, Smith N F, Eaton W P, Miller W M, Miller S L. The effect of humidity on the reliability of a surface micromachined microengine. In *IEEE International Reliability Physics Symposium,* San Diego, 1999: 189–197.

[11] Henck S A. Lubrication of digital micromirror devices ™. *Tribol Lett* **3**: 239–247 (1997)

[12] Asay D B, Dugger M T, Kim S H. *In-situ* vapor-phase lubrication of MEMS. *Tribol Lett* **29**: 67–74 (2008)

[13] Meyer E, Overney R, Brodbeck D, Howald L, Lüthi R, Frommer J, Güntherodt H-J. Friction and wear of Langmuir-Blodgett films observed by friction force microscopy. *Phys Rev Lett* **69**: 1777–1780 (1992)

[14] Liu F, Laboriante I, Bush B, Roper C S, Carraro C, Maboudian R. *In situ* studies of interfacial contact evolution via a two-axis deflecting cantilever microinstrument. *Appl Phys Lett* **95**: 131902–131904 (2009)

[15] Merkle A P, Marks L D. Friction in full view. *Appl Phys Lett* **90**: 064101–064103 (2007)

[16] Alsem D H, Dugger M T, Stach E A, Ritch R O. Micron-scale friction and sliding wear of polycrystalline silicon thin structural films in ambient air. *J Microelectromech S* **17**: 1144–1154 (2008)

[17] Gotsmann B, Lantz M A. Atomistic wear in a single asperity sliding contact. *Phys Rev Lett* **101**: 125501–125504 (2008)

[18] Archard J F. Contact and rubbing of flat surfaces. *J Appl Phys* **24**: 981–988 (1953)

[19] Timpe S J, Alsem D H, Hook D A, Dugger M T, Komvopoulos K. Wear of polysilicon surface micromachines operated in high vacuum. *J Microelectromech S* **18**: 229–238 (2009)

[20] Hagedorn P. *Non-linear Oscillations*. Oxford (UK): Clarendon Press, 1981.

[21] Nakayama K, Zhang L. Work function of scratched silicon surface during $O_2$ and $N_2$ adsorption. *Jpn J Appl Phys* **39**: 4509–4511 (2000)

[22] Mate C M. *Tribology on the Small Scale*. Oxford (UK): Oxford University Press, 2008.

[23] Mo Y, Turner K T, Szlufarska I. Friction laws at the nanoscale. *Nature* **457**: 1116–1119 (2009)

[24] Ciraci S, Wagner H. Dissociation of water molecules on Si surfaces. *Phys Rev B* **27**: 5180–5183 (1983)

[25] Eng Jr J, Raghavachari K, Struck L M, Chabal Y J, Bent B E, Flynn G W, Christman S B, Chaban E E, Williams G P, Radermacher K, Mantl S. A vibrational study of ethanol adsorption on Si (100). *J Chem Phys* **106**: 9889–9898 (1997)

[26] Helt J M, Batteas J D. Wear of mica under aqueous environments: Direct observation of defect nucleation by AFM. *Langmuir* **21**: 633–639 (2005)

[27] Strawhecker K, Asay D B, Kim S H. Gas-phase lubrication of mems devices: Using alcohol vapor adsorption isotherm for lubrication of silicon oxides. In *Encyclopedia of chemical processing*. Lee S, Ed. New York: Taylor and Francis, 2006, **2**: 1143–1150.

[28] Shen S H, Meng Y G, Zhang W. Characteristics of the wear process of side-wall surfaces in bulk-fabricated Si-MEMS devices in nitrogen gas environment. *Tribol Lett* **47**: 455–466 (2012)

[29] Asay D B, Kim S H. Evolution of the adsorbed water layer structure on silicon oxide at room temperature. *J Phys Chem B* **109**: 16760–16763 (2005)

[30] Barnette A L, Asay D B, Kim D, Guyer B D, Lim H, Janik M J, Kim S H. Experimental and density functional theory study of the tribochemical wear behavior of $SiO_2$ in humid and alcohol vapor environments. *Langmuir* **25**: 13052–13060 (2009)

**Sihan Shen** received his Bachelor degree in Mechanical Engineering in 2006 from Tsinghua University, Beijng, China. After then, he was a Ph.D student in the State Key Laboratory of Tribology at the same university. He has recently obtained his Ph.D. degree in Mechanical Engineering at Tsinghua University. His research interests include microelectromechanical systems and microtribology.

**Yonggang Meng** received his M.S. and Ph.D degrees in Mechanical Engineering from Kumamoto University, Japan, in 1986 and 1989 respectively. He joined the State Key Laboratory of Tribology at Tsinghua University from 1990. His current position is a Professor and the Deputy Director of the laboratory. His research areas cover the tribology of MEMS and Hard Disk Drives, active control of friction and interfacial phenomena and nanomanufacturing.